Mathematical Modeling and Analysis of Aerodynamic and Thermal Effects on the Descent Module of the Spacecraft *ExoMars-2020* During Soft Landing

A. V. Babakov[a], * and S. I. Shmatov[b], **

[a] Institute for Computer-Aided Design Russian Academy of Sciences, Moscow, Russia
[b] Lavochkin Association, Khimki, Moscow oblast, Russia
*e-mail: avbabakov@mail.ru
**e-mail: shmatovsi@laspace.ru

Abstract—Results of a numerical study of the flow structure occurring between the descent module and landing surface during the braking maneuver of the propulsion system are presented. Data on the force and thermal effect of the emerging flow on the descent module are given, depending on its distance and orientation relative to the landing surface and amount of the braking engine thrust. The pictures of the arising unsteady vortex motion of the medium are presented.

Keywords: spacecraft, descent module, soft landing, aerodynamics, unsteady flow, numerical modeling, flow pattern, vortex flows

DOI: 10.1134/S0038094621070042

INTRODUCTION

The study of the planets of the Solar System and especially the terrestrial planets and their satellites, which began in the 60s of the last century, continues to be one of the main tasks of world cosmonautics (Efanov and Shirshakov, 2018). Moreover, along with scientific research, this study is acquiring more and more practical interest. The success of solving these problems largely depends on the reliability of technologies for landing spacecraft (SC) on the surface of the celestial body under study. For high-quality design and successful operation of modern descent modules (DMs), it is necessary not only to have sufficiently accurate information on the integral power, torque and thermal characteristics of the impact on the elements of the DM structure, but also detailed information on the flow structure around the DM and the landing surface (LS).

In the 70s and 80s of the last century, numerical results were obtained (Golomazov et al., 1982; Dubinskaya and Ivanov, 1976), which revealed a number of characteristic features of the interaction of single streamflows with an obstacle, and in good agreement with the corresponding experimental data (Golubkov et al., 1972; Lunev et al., 1971; Melnikova and Nesterov, 1971).

On modern DMs and reentry vehicles (RVs), braking propulsion systems (BPSs) have a multinozzle configuration, which leads to a substantially three-dimensional and unsteady nature of the flow arising during DM and RV landing. Accordingly, the problem of numerical modeling of such a flow should be considered in a three-dimensional formulation. All this significantly complicates the problem compared to the case of a single jet stream and requires a multiple increase in computational resources. Therefore, the problems of the interaction of multiblock jets with obstacles, despite the demand, remain insufficiently studied. And often when developing a DM, especially in the early stages of design, approximate engineering techniques are used to quickly obtain preliminary estimates of the force impact of jets on the DM and LS (Shmatov, 2017). To obtain more complete and accurate information on the characteristics of the flow near specific DMs and LSs, either a ground-based experimental study of the DM is required (Kudimov et al., 2013; Makarov et al., 2014), or numerical simulation in full staging for each specific project. Recognizing the importance of experimental studies, it should be noted that for the problem under consideration, the manufacture of models, the preparation of equipment and the conduct of the research itself require a large expenditure of money and time, which greatly increases the cost of work and reduces their efficiency
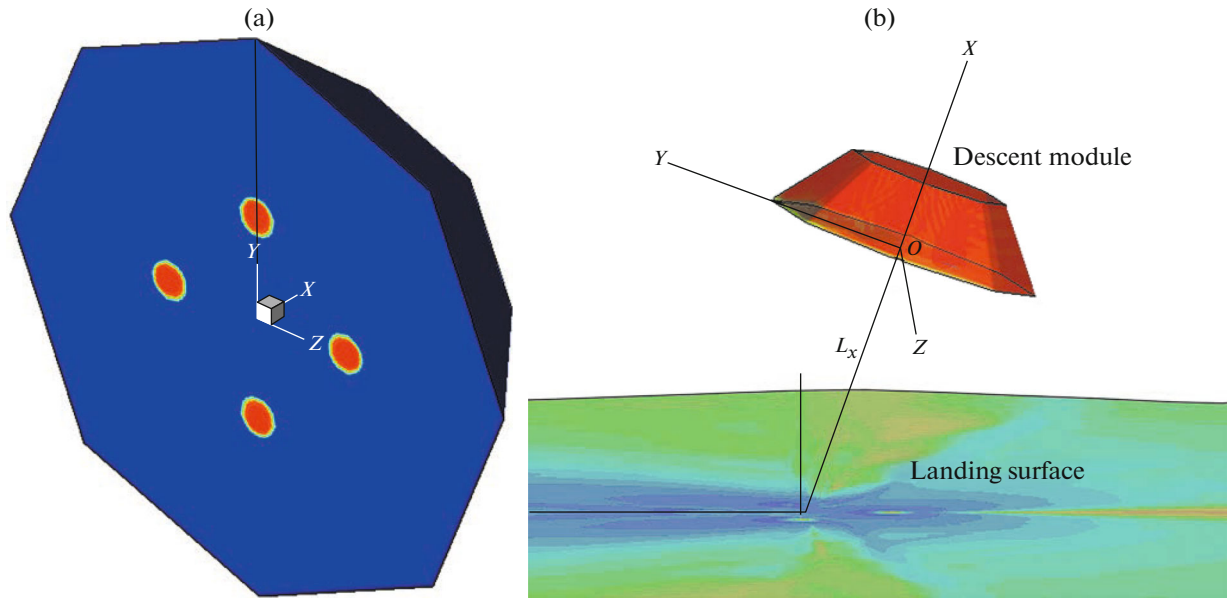
Fig. 1. The coordinate system used with the designations (a) and the shape of the landing module (b).

in comparison with even the most costly numerical calculations.

The level of modern supercomputers, numerical methods and technologies of high-performance computing makes it possible to carry out numerical modeling of such spatially unsteady flows with an accuracy satisfactory for designers and within an acceptable time, as evidenced by (Babakov et al., 2015; Glazunov et al., 2014).

This paper presents a three-dimensional nonstationary formulation and results of a numerical solution of the problem of the interaction of a four-block supersonic jet BPS with the landing surface when *ExoMars-2020* is landing under Martian atmospheric conditions.

1. NUMERICAL TECHNIQUE

Numerical calculations were carried out on the basis of the FLUX software package (Babakov, 2016), based on the conservative numerical method of flows (Babakov et al., 1975; Belotserkovsky and Severinov, 1973). The method and software package are designed to study the spatially unsteady motion of a compressible medium at sub-, trans-, and supersonic speeds. Previously, the complex was used to simulate the aerodynamics of descent vehicles (Babakov et al., 2014; Babakov and Finchenko, 2019; Belotserkovsky et al., 2016) and soft landing (Babakov et al., 2015).

The software package is based on parallel algorithms of the method and is implemented on modern supercomputer systems of cluster architecture. The

computing complex used in the calculations performs at 181 TFlops and has an operative memory of 17408 GB.

2. PROBLEM STATEMENT

Numerical modeling of the motion of an inviscid compressible gaseous medium near the DM and LS, arising from the interaction of the BPS jets with the atmospheric medium and a solid surface, is considered. The medium is heterogeneous, consisting of two chemically nonreactive gases with different thermodynamic properties: atmospheric gas and BPS gas. Modeling is carried out in a three-dimensional nonstationary setting.

Figure 1a shows the right-handed coordinate system $OXYZ$ associated with the DM and the notation adopted.

The simplified form of the DM is a regular truncated octagonal pyramid (Fig. 1b). In the calculations, the following geometric dimensions of the DM were taken: the radius of the circle described near the frontal face $R_0 = 1.695$ m; the radius of the circle described near the bottom edge $R_1 = 0.981$ m; and the distance between the frontal and bottom edges is $L = 0.912$ m.

The scheme of the BPS nozzles is also shown in Fig. 1b. The BPS nozzles are placed evenly around the circumference of the radius $R_a = 0.601$ m, the cutoff radius of the BPS nozzles is $r_a = 0.096975$ m. The half-opening angle of the BPS nozzles β was 10°. The slope δ of the axes of the BPS nozzles to the DM axis was 7°. The geometric parameters of the BPS and the location of the nozzles were chosen close to those presented in (Aleksandrov et al., 2014). The velocity vector at the

exit of each nozzle was assumed to be constant in absolute value, but changing in direction depending on the distance from the axis of a particular nozzle.

The calculations were carried out on the basis of parallel algorithms using up to 1000 computational cores. Spatial computational grids included up to 20 million finite volumes and were characterized by exponential compression to the frontal, lateral and bottom surfaces of the DM, as well as to the regions of propagation of the BPS jets.

The initial fields of the gas-dynamic parameters at time $t = 0$ in the entire region of integration correspond to the parameters of the atmospheric gas. The atmosphere is assumed to be unperturbed with zero velocities in the entire region of integration. On the sections of the BPS nozzles, the dynamic and gas-dynamic parameters corresponding to the operational mode of the BPS are set.

3. CALCULATION RESULTS

Numerical calculations were carried out for different distances L_x and angles α of the DM tilt relative to the LS in two modes of operation of the BPS, corresponding to the minimum and maximum values of thrust (Likhachev and Fedotov, 2014).

The calculations were performed for the following values of atmospheric gas parameters: temperature $T_H = 225.6$ K, pressure $P_H = 586.72$ Pa, density $\rho_H = 0.01364$ kg/m^3, ratio of specific heat capacities $\gamma_H = 1.329$, and molecular weight $\mu_H = 0.0436$ kg/mol.

In mode 1, the thrust of the BPS (in vacuum) was $G_{min} = 1947.0$ N, the flow rate was $N_1 = 0.9$ kg/s. In this case, the parameters at the sections of the BPS nozzles had the following values: temperature $T_A = 219.0$ K, pressure $P_A = 510$ Pa, density $\rho_A = 0.003633$ kg/m^3, ratio of specific heat capacities $\gamma_A = 1.3372$, molecular weight $\mu_A = 0.01297$ kg/mol, Mach number per cross-section of the BPS nozzles $M_A = 4.915$, and the modulus of velocity at the cross-section of the BPS nozzles $V_A = 2129.0$ m/s.

In mode 2, the thrust of the BPS (in vacuum) and the flow rate had significantly higher values and were, respectively: $G_{max} = 13637.0$ N and $N_2 = 6.22$ kg/s. In this case, the parameters at the sections of the BPS nozzles had the following values: temperature $T_A = 319.5$ K, pressure $P_A = 4450$ Pa, density $\rho_A = 0.02499$ kg/m^3, ratio of specific heat capacities $\gamma_A = 1.2922$, molecular weight $\mu_A = 0.01492$ kg/mol, Mach number per the section of the BPS nozzles $M_A = 4.46$, the modulus of the velocity at the edges of the BPS nozzles $V_A = 2139.0$ m/s.

For the indicated operating modes of the BPS, numerical calculations were carried out for three values of the angle of inclination of the DM axis to the LS: $\alpha = 0°$, $10°$, and $20°$ at a fixed distance between the DM and the LS $L_x = 2R_0$, as well as at a zero value of the inclination angle of the DM axis to the LS for two other values of the distance between DM and LS: $L_x = 3R_0$ and $L_x = 4R_0$.

In what follows, dimensionless variables are used (the corresponding dimensional values are given in brackets, if necessary). In this case, the linear dimensions are related to the radius R_0, the density and temperature are related to the corresponding parameters ρ_H and T_H in atmospheric gas, the velocities to the speed of sound in atmospheric gas a_H, pressure to $\rho_H a_H^2$, and thrust and force characteristics to $\rho_H a_H^2 R_0^2$. Time is referred to $t_0 = R_0/a_H$. For the calculations considered below, $a_H = 239.1$ m/s and $t_0 = 7.089 \times 10^{-3}$ s. The pitching moment Mz was calculated relative to the point with coordinates $X_c = Y_c = Z_c = 0.000$.

3.1. General Picture of the Flow

Let us first consider the nature of the flow arising between the DM and the LS using the example of a calculation with the following parameter values: the distance between the DM and the LS $L_x = 2R_0$, the angle of inclination of the DM to the LS $\alpha = 20°$, and thrust $G = G_{min}$.

Figure 2 for the time instant $t = 20$ (0.142 s) after switching on the BPS engines shows the gas density isosurfaces of the BPS at a level of 10% of the BPS gas density at the nozzle sections and instant streamlines constructed from points located in the OYZ plane.

These pictures indicate the development of an unsteady vortex flow between the DM and LS, caused by the jets of the BPS. In the process of numerical calculations, the flow near the DM reaches a steady-state (in the sense of time-averaged values of gas-dynamic parameters), but a nonstationary mode. The arising vortex motion is characteristic of all the design options considered below and happens at times longer ~50–100 (~0.3–0.7 s).

3.2. Calculations at Various Inclination Angles of the DM to the LS

Calculations were carried out for two values of the TPS thrust: $G = G_{min}$ and $G = G_{max}$ at the distance between the DM and the LS $L_x = 2R_0$ and three values of the inclination angle of the DM axis to the LS: $\alpha = 0°$, $10°$, and $20°$.

3.2.1. Calculations with thrust value $G = G_{min}$. In the calculations performed, the flow between the DM
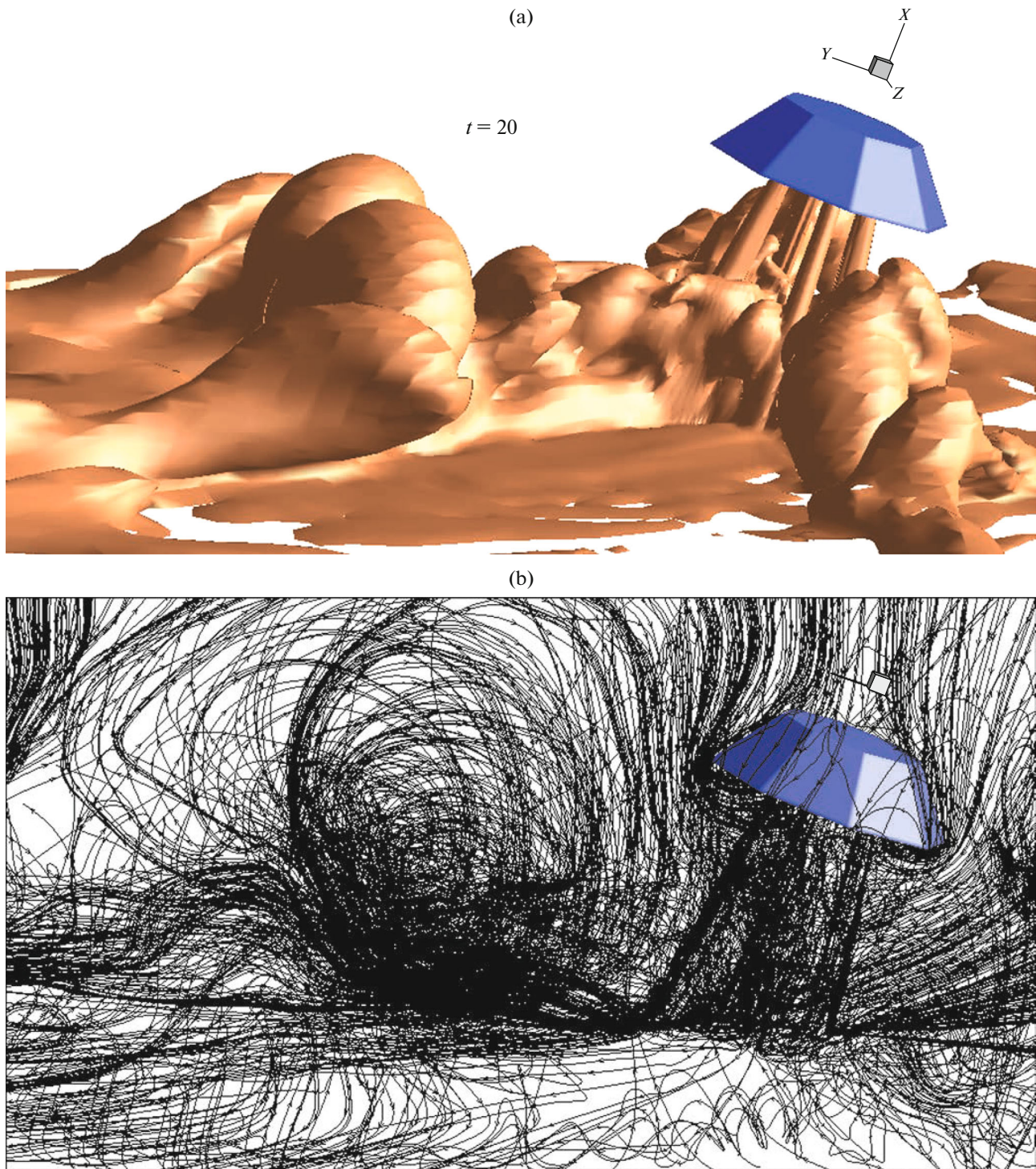
Fig. 2. Density isosurfaces of gases BPS (a) and instantaneous streamlines (b) at time $t = 20$ (0.142 s).

and LS is nonstationary. This is indicated by the time dependences of the longitudinal force Fx and the pitching moment Mz shown in Fig. 3.

The observed oscillations of the longitudinal force and pitching moment are associated with the influence on the frontal surface of the DM of the nonstationary interaction of the supersonic jets of the BPS with the LS.

Figure 4 shows the temperature fields in the OXY plane, on the LS, as well as on the frontal surface of the DM at different inclination angles of the DM to the LS.
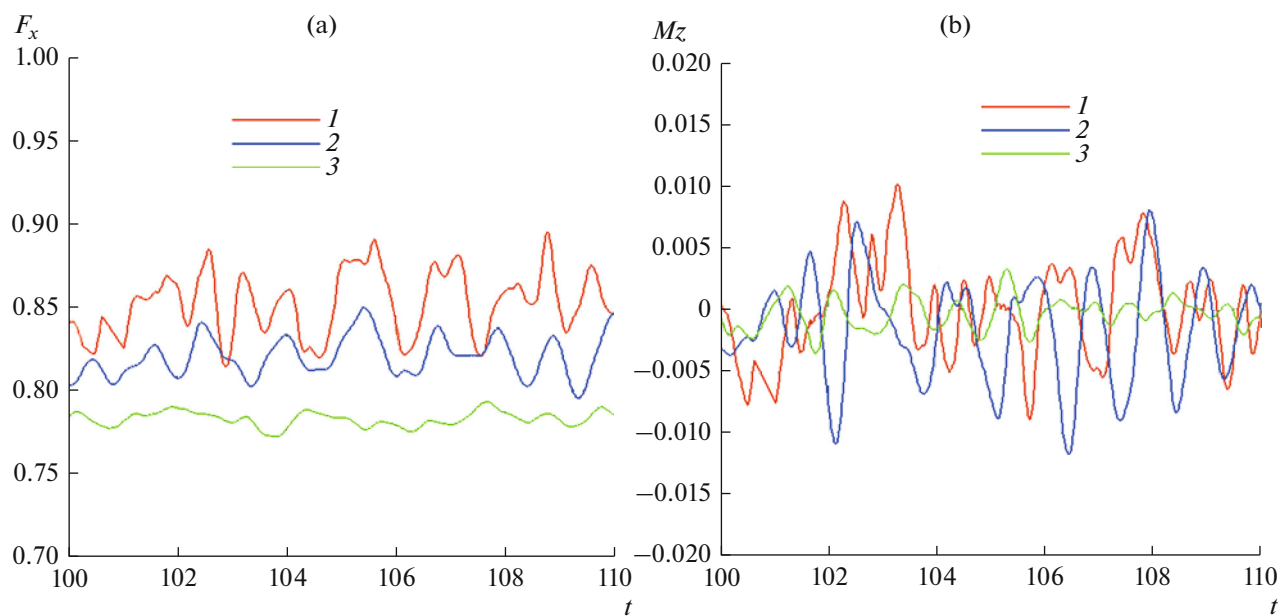
Fig. 3. Time behavior of the longitudinal force Fx (a) and the pitching moment Mz (b) at different inclination angles of the DM to the LS. (*1*) $\alpha = 0°$; (*2*) $\alpha = 10°$; (*3*) $\alpha = 20°$.
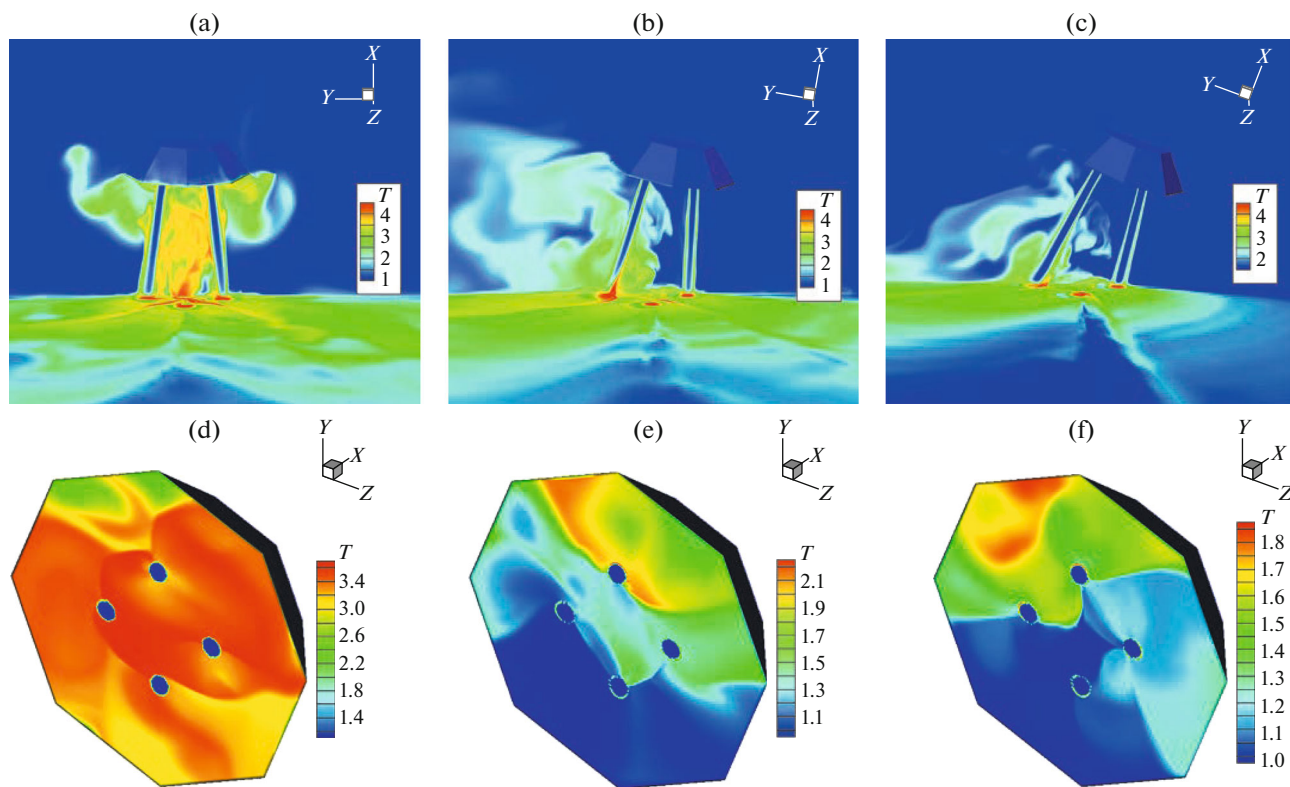
Fig. 4. Temperature fields in the plane OXY and on the LS (a, b, c) and on the frontal surface of the DM (d, e, f) at different inclination angles of the DM to the LS. (a, d) $\alpha = 0°$; (b, e) $\alpha = 10°$; (c, f) $\alpha = 20°$.

Table 1. Time-averaged values of the ratio of the longitudinal force Fx to the thrust G, the pitching moment Mz, and the value of the maximum temperature T_{max} on the DM surface at different angles of inclination of the DM to the LS

α	0°	10°	20°
Fx/G	0.976	0.942	0.902
Mz	0	−0.002	−0.0007
T_{max}	3.98 (898 K)	2.32 (523 K)	1.91 (431 K)

Table 2. Time-averaged values of the ratio of the longitudinal force Fx to the thrust value $G = G_{max}$ and the maximum temperature T_{max} on the DM surface at different inclination angles of the DM to the LS

α	0°	10°	20°
Fx/G	1.007	0.976	0.929
T_{max}	5.91 (1333 K)	5.56 (1254 K)	3.25 (733 K)

Figure 4 shows that, at $\alpha = 0°$, the BPS gas reflected from the LS propagates up to the frontal surface of the DM. The flow near the DM frontal surface is also nonstationary. This is indicated by the temperature fields on the frontal surface of the DM.

Table 1 shows the time-averaged values of the ratio of the longitudinal force Fx to the thrust $G = G_{min}$, the pitching moment Mz, and the values of the maximum temperature T_{max} on the DM surface at various angles of inclination of the DM to the LS. Hereinafter, averaging over time was carried out for a flow regime established near the DM in the time interval $\Delta = 100$.

3.2.2. Calculations with thrust value $G = G_{max}$. Below are the results of calculations obtained for the thrust value $G = G_{max}$, which is significantly greater than that considered above, and for the distance between the DM and the LS $L_x = 2R_0$.

Figure 5 shows the temperature fields in the OXY plane (a, b, c) and on the DM frontal surface (d, e, f), similar to those shown in Fig. 4 for $G = G_{min}$.

For the considered value of the BPS thrust, significant fluctuations of the longitudinal force Fx and the pitching moment Mz are observed, Fig. 6.

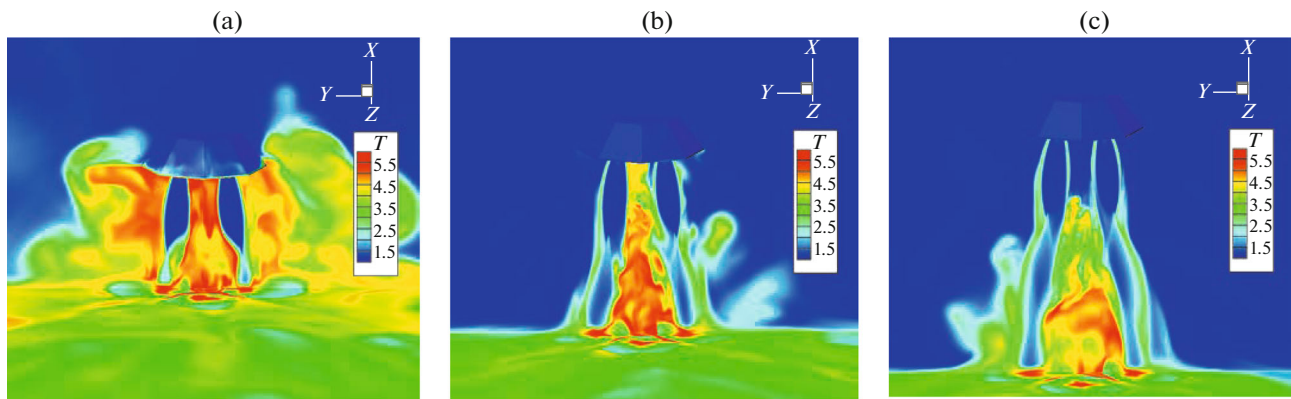Table 2 shows the time-averaged values of the ratio of the longitudinal force Fx to the thrust value $G = G_{max}$ and the maximum gas temperature T_{max} on the DM surface at various inclination angles of the DM to the LS.
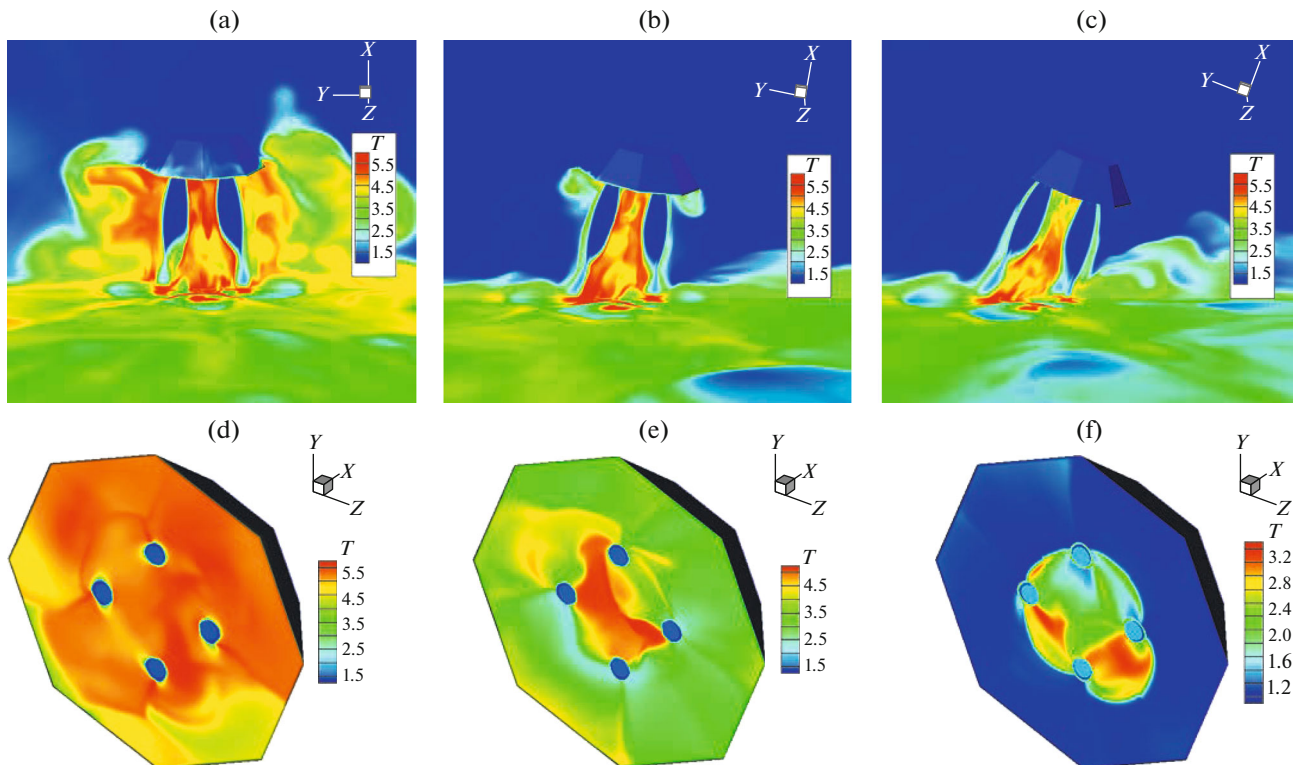
Fig. 5. Temperature fields in the plane OXY and on the LS (a, b, c) and on the frontal surface of the DM (d, e, f) at different inclination angles of the DM to the LS. (a, d) $\alpha = 0°$; (b, e) $\alpha = 10°$; (c, f) $\alpha = 20°$.
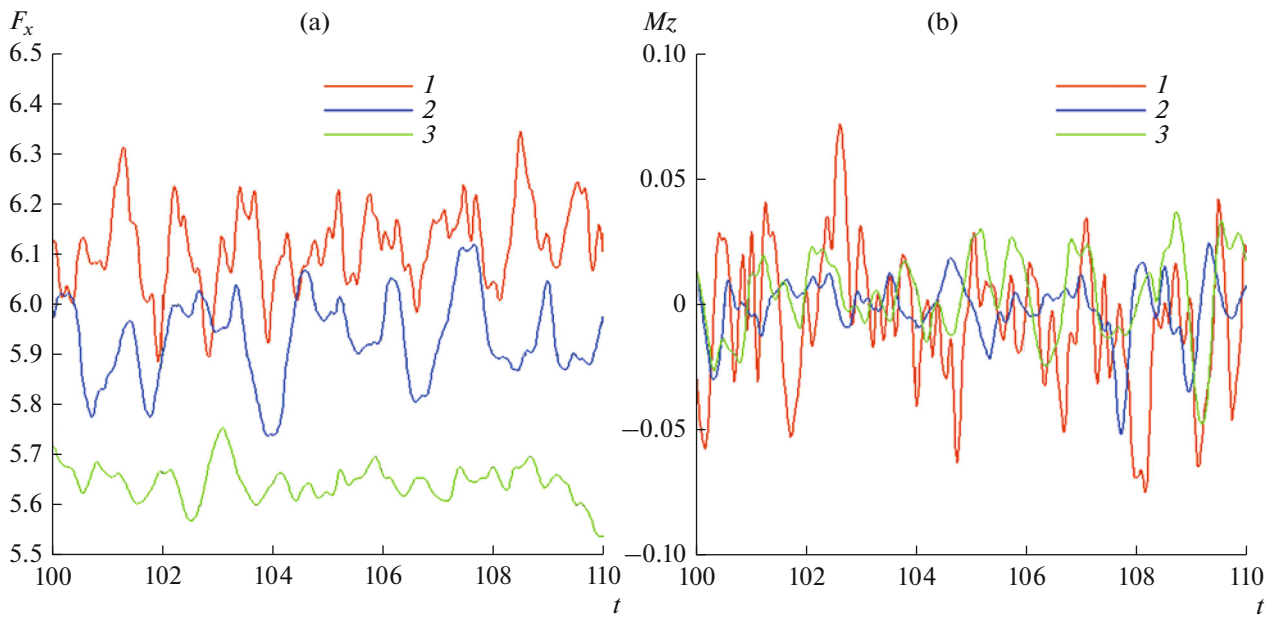
Fig. 6. Time behavior of the longitudinal force Fx (a) and the pitching moment Mz (b) at different inclination angles of the DM to the LS. (*1*) $\alpha = 0°$; (*2*) $\alpha = 10°$; (*3*) $\alpha = 20°$.

Fig. 7. Temperature fields in the OXY plane and on the LS at different distances between the DM and the LS. (a) $L_x = 2R_0$; (b) $L_x = 3R_0$; (c) $L_x = 4R_0$.

3.3. Calculations at Various Distances Between the DM and the LS

Below are the results of calculations for the distances between the DM and the LS $L_x = 2R_0$, $3R_0$, and

Table 3. Time-averaged values of the ratio of the longitudinal force Fx to the thrust value $G = G_{max}$ and the maximum temperature T_{max} on the DM surface at different distances between the DM and the LS

L_x	$2R_0$	$3R_0$	$4R_0$
Fx/G	1.007	0.990	0.989
T_{max}	5.91 (1333 K)	4.74 (1069 K)	3.25 (733 K)

$4R_0$ with the thrust value $G = G_{max}$ and a zero inclination angle of the DM to the LS ($\alpha = 0°$).

The temperature fields shown in Fig. 7 in the OXY plane and on the frontal surface of the DM for different distances between the DM and the LS give an idea of the nature of the flow between the DM and the LS.

At the indicated distances between the DM and the LS, the unsteadiness of the flow arising between the DM and the LS, as in the calculations presented above, leads to pulsations of the force action of the flow on the DM.

Table 3 shows the time-averaged values of the ratio of the longitudinal force Fx to the thrust value $G = G_{max}$ and the maximum temperature T_{max} on the DM surface at various distances between the DM and the LS.

CONCLUSIONS

As a result of numerical modeling of the above problem in a three-dimensional nonstationary formulation, a number of factors were identified that can have a noticeable negative effect on the functional state of the scientific and service equipment that is part of the DM, as well as on the gas and dust environment in the vicinity of the landing site. So, depending on the distance of the DM from the LS, the orientation of the DM relative to the LS, the mode of operation of the BPS, the loss of the braking effect can reach 10% of the BPS thrust.

Under certain operating modes of the BPS near the LS, the BPS jets reflected from it can have a significant thermal effect on the DM; on its frontal surface, zones of high gas temperature exceeding 1300 K may appear.

The results of numerical modeling also indicate a substantially unsteady vortex flow between the DM and the LS, which leads to pulsations of the force action on the DM and the formation of dust clouds that disrupt the operation of devices and special equipment on the DM.

Identification and study of the listed negative factors is necessary for the design and implementation of more advanced DMs and BPSs.

Thus, the presented results show the capabilities of the FLUX program complex implemented on the supercomputer when carrying out a numerical study of the flow structure and its effect on the DM during landing with an operating BPS.

Moreover, the availability of such a computing tool can play an important role in solving similar urgent problems. Such, for example, as determining the force effect of jets of low-thrust engines of the control system on the structural elements of spacecraft and determining the degree of pollution in the vicinity of sensitive devices.

REFERENCES

Aleksandrov, L.G., Morozov, V.I., Stepanov, S.S., et al., Propulsion system of the descent module landing platform, *Vestn. NPO im. S.A. Lavochkina*, 2014, no. 2, pp. 116−119.

Babakov, A.V., Program package FLUX for the simulation of fundamental and applied problems of fluid dynamics, *Comput. Math. Math. Phys.*, 2016, vol. 56, no. 6, pp. 1151−1161.

Babakov, A.V. and Finchenko, V.S., The numerical simulation of aerodynamics of the frontal aerodynamic screen of ExoMars project descent vehicle and the analysis of flow pattern in the base area and near wake, *Sol. Syst. Res.*, 2019, vol. 54, no. 7, pp. 712−718.

Babakov, A.V., Belotserkovskii, O.M., and Severinov, L.I., Numerical investigation of the flow of a viscous heat-conducting gas near a blunt body of finite dimensions, *Fluid Dyn.*, 1975, vol. 10, no. 3, pp. 457−466.

Babakov, A.V., Beloshitskii, A.V., Gaidaenko, V.I., and Dyad'kin, A.A., Calculation by the flow method of the flow structure and aerodynamic characteristics when separating the frontal heat shield from the reentry vehicle, *Kosm. Tekh. Tekhnol.*, 2014, no. 4, pp. 20−25.

Babakov, A.V., Beloshitskii, A.V., Gaidaenko, V.I., and Dyad'kin, A.A., Numerical simulation and analysis of flow patterns near a reentry space vehicle with firing rocket engines in the vicinity of the landing surface, *Kosm. Tekh. Tekhnol.*, 2015, no. 4, pp. 1−8.

Belotserkovskii, O.M. and Severinov, L.I., The conservative "flow" method and the calculation of the flow of a viscous heat-conducting gas past a body of finite size, *USSR Comput. Math. Math. Phys.*, 1973, vol. 13, no. 2, pp. 141−156.

Belotserkovskii, O.M., Babakov, A.V., Beloshitskiy, A.V., Gaydaenko, V.I., et al., Numerical simulation of some problems of recovery capsule aerodynamics, *Math. Model. Comput. Simul.*, 2016, vol. 8, no. 5, pp. 568−576.

Dubinskaya, N.V. and Ivanov, M.Ya., Numerical study of stationary regimes of interaction of a supersonic underexpanded jet with a flat obstacle located perpendicular to its axis, *Izv. Akad. Nauk SSSR, Mekh. Zhidk. Gaza*, 1976, no. 5, pp. 49−57.

Efanov, V.V. and Shirshakov, A.E., Studies of Mars and its satellites by advanced interplanetary stations designed by the Lavochkin Association (On the thirtieth anniversary of the launch of the *Phobos-2* spacecraft), *Sol. Syst. Res.*, 2018, vol. 53, no. 7, pp. 487−492.

Glazunov, A.A., Kagenov, A.M., Eremin, I.V., and Kuvshinov, N.E., Numerical study of the interaction of combustion products of spacecraft engines with streamlined surfaces in the conditions of Mars, *Izv. Vyssh. Uchebn. Zaved., Fiz.,* 2014, vol. 57, no. 8/2, pp. 97−103.

Golomazov, M.M., Davydov, Yu.M., Ezhkov, V.V., and Shmatov, S.I., Study of flow fields in the region of interaction of a supersonic underexpanded jet with obstacles, *Izv. Akad. Nauk SSSR, Mekh. Zhidk. Gaza*, 1982, no. 3, pp. 181−184.

Golubkov, A.G., Koz'menko, B.K., Ostapenko, V.A., and Solotchin, A.V., Interaction of a supersonic underexpanded jet with a plane bounded obstacle, *Izv. Sib. Otd. Akad. Nauk SSSR, Ser. Tekh. Nauk,* 1972, vol. 13, no. 3, pp. 52−60.

Kudimov, N.F., Safronov, A.V., and Tret'yakova, O.N., Results of experimental studies of the interaction of multi-block supersonic turbulent jets with an obstacle, *Tr. Mosk. Aviats. Inst.*, 2013, no. 69. http://trudy-mai.ru/published.php?ID=43076. Accessed June 17, 2020.

Likhachev, V.N. and Fedotov, V.P., Control of the movement of the lander of the EXOMARS spacecraft at the stage of descent and landing on the surface of Mars, *Vestn. NPO im. S.A. Lavochkina*, 2014, no. 2, pp. 58–64.

Lunev, V.V., Gubanova, O.I., and Plastinina, L.I., On the central stall zone in the interaction of a supersonic underexpanded jet with an obstacle, *Izv. Akad. Nauk SSSR, Mekh. Zhidk. Gaza*, 1971, no. 2, pp. 135–138.

Makarov, V.P., Biryukov, A.S., Mikhailov, D.N., and Aleksandrov, L.G., Selected aspects of ground-based experimental testing of the EXOMARS-2018 spacecraft, *Vestn. NPO im. S.A. Lavochkina*, 2014, no. 2, pp. 124–127.

Mel'nikova, M.F. and Nesterov, Yu.N., Impact of a supersonic off-design jet on a flat obstacle perpendicular to the jet axis, *Uch. Zap. – Tsentr. Aerogidrodin. Inst.*, 1971, vol. 2, no. 5, pp. 44–58.

Shmatov, S.I., Methodology for engineering calculation of the force effect of supersonic jets emanating from low-thrust engines on structural elements of spacecraft in inviscid approximation, *Vestn. NPO im. S.A. Lavochkina*, 2017, no. 4, pp. 145–152.

Translated by E. Seifina